Appl. Phys. B 76, 393–396 (2003)
DOI: 10.1007/s00340-003-1136-4

Applied Physics B
Lasers and Optics

M.C. WENGLER✉
M. MÜLLER
E. SOERGEL
K. BUSE

Poling dynamics of lithium niobate crystals

University of Bonn, Institute of Physics, Wegelerstr. 8, 53115 Bonn, Germany

Received: 6 February 2003
Published online: 9 April 2003 •

ABSTRACT Ferroelectric domain reversal via electric field poling of congruently melting lithium niobate ($LiNbO_3$) crystals is investigated. An electro-optic interferometric observation technique reveals spatial and temporal dynamics of the poling process. Starting from seeds, the domains grow until the entire crystal has a switched polarization. During the switching process the boundaries are preferentially aligned along the crystallographic axes. The coercive field between two sequenced domain inversions is transiently reduced after a poling event, and recovers exponentially with a time constant of about half a minute. No light-induced change of the recovery time constant, neither with green nor with ultraviolet light, is observed. The results are of relevance for domain engineering of $LiNbO_3$ crystals.

PACS 42.70.Mp; 77.80.Fm

1 Introduction

The fabrication of periodically poled lithium niobate (PPLN) crystals is of interest for various applications. Using the material's nonlinear and electro-optic properties, devices such as frequency doublers [1, 2], optical parametric oscillators (OPOs) [3–5] or electro-optic Bragg reflectors [6] can be made. So far, PPLN with period lengths down to 4 μm is available [7]. However, smaller structures (< 0.5 μm) are required for many applications, for example for electro-optically switchable Bragg-reflection gratings in telecommunication.

Domain inversion can be achieved by electric field poling. An electric field is applied along the c axis of a crystal. If this field exceeds a certain value, the so-called coercive field, the ferroelectric domains will be inverted. Electric field poling via structured electrodes is the conventional method of fabricating periodically poled lithium niobate ($LiNbO_3$) and lithium tantalate ($LiTaO_3$) crystals [8]. The major limitation is the minimal period length achievable with this method due to inhomogeneities of the electric field. Spatial modification of the poling characteristics of the material rather than structuring the electric field can avoid such limitations. The coercive field of $LiTaO_3$ shows a recovery behavior between two successive domain inversions, i.e. for some time after the poling the coercive field is lowered and thus the domains can be switched back to the original state with a smaller field [9]. The recovery time constant can be influenced by light: the coercive field of $LiTaO_3$ shows a faster recovery in illuminated areas than in dark regions. Using two successive domain inversions, it is possible to achieve light-frustrated poling [10]. Utilizing this method, periodic domain inversion with a period length of 6.3 μm has been realized in $LiTaO_3$ [11]. $LiNbO_3$ is an isomorphic material to $LiTaO_3$ and should exhibit similar characteristics. However, light-frustrated poling has not been shown in $LiNbO_3$ so far.

We present investigations of the poling dynamics of $LiNbO_3$ and of our attempts at light-frustrated domain patterning.

✉ Fax: +49-228/734038, E-mail: wengler@physik.uni-bonn.de

2 Methods

Congruently melting, z-cut $LiNbO_3$ crystals ($15 \times 15 \times 0.5\,mm^3$, Crystal Technologies, Inc.) are used in all experiments. For domain inversion an electric field that exceeds the coercive field E_c must be applied along the c axis. The poling direction of a virgin crystal is called 'forward poling', while the opposite direction is called 'reverse poling'. It is known that the coercive fields for forward poling ($E_{c,f}$) and for reverse poling ($E_{c,r}$) have different values [11].

Figure 1 shows the sample holder used for poling experiments. The electric field is applied to the crystal using transparent liquid electrodes (water), which allow illumination during the poling experiments. Furthermore, the liquid electrodes lead to a very homogeneous electric field within the crystal due to their perfect attachment to the crystal surface. The electrical connection to the high-voltage supply includes a 50-MΩ safety resistor.

In our poling experiments, the applied voltage is ramped linearly with time (15 V/s). When the electric field reaches or exceeds the coercive field, domain inversion starts. Due to charge redistribution within the crystal structure a displacement current (or poling current) occurs. From this current information about the temporal dynamics of the poling process is obtained.

An additional method of in situ observation of poling processes is an electro-optic interferometric technique. The

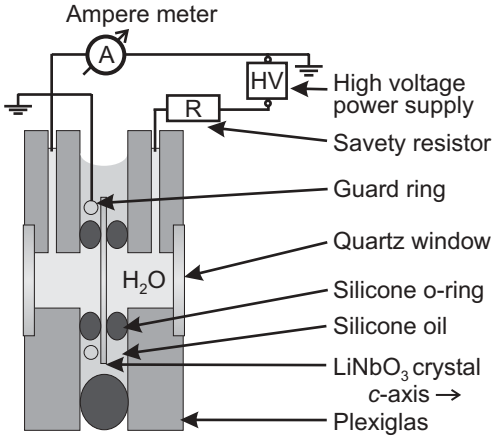

FIGURE 1 Schematic drawing of the sample holder used for poling experiments: the z-cut $LiNbO_3$ crystal is pressed between two silicone o-rings. Liquid electrodes (water) within these o-rings are used to apply a homogeneous electric field. Leakage currents are suppressed by the surrounding silicone oil or grounded by the guard ring. Quartz windows allow illumination of the crystal with visible or ultraviolet light. A high-voltage power supply (HV) is electrically connected to the water electrodes. An ampere meter (A) measures the displacement current. The resistor ($R = 50\,\mathrm{M\Omega}$) is included for safety reasons

refractive-index change due to the electro-optic effect depends on the domain orientation ($\Delta n \propto r_{13} E_3$). By positioning the poling setup in a Mach–Zehnder interferometer as shown in Fig. 2, the domain walls become visible in the interference pattern when a voltage is applied. With this setup it is possible to investigate the temporal and spatial behavior of the poling process. Additionally, pump light can be directed onto the crystal by dielectric mirrors to investigate the influence of light on the poling process. The interference pattern can be observed either at a single point with a photodiode or as a whole image on the screen. A video camera is used to obtain a movie of the poling process.

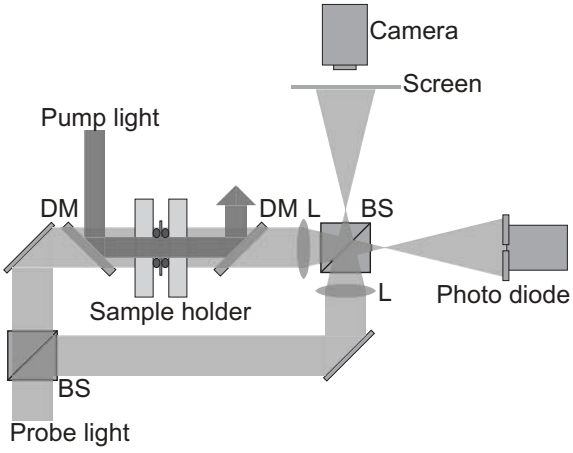

FIGURE 2 Schematic drawing of the poling setup within a Mach–Zehnder interferometer. BS, beam splitter; DM, dielectric mirror; L, lens. On the screen, the whole interference pattern can be observed, while the photodiode measures the intensity of a single point of the interference pattern. When applying a voltage to the crystal, the refractive-index change due to the electro-optic effect depends on the domain orientation, and the domain pattern becomes visible on the screen. A poling video can be obtained with a camera. By using dielectric mirrors, pump light of a different wavelength can be directed onto the crystal, and light-induced effects can be investigated

To measure the coercive field of the sample, either the displacement current or the interference signal can be used. The moment when the domains are switched is determined, and the voltage that is applied at this time defines the coercive field. To investigate a transient reduction of the coercive field after a poling event, we use poling cycles: the crystal is poled in one direction and, then, after a recovery time t_r, it is poled back to the original direction. The influence of light (wavelength λ, intensity I) on the coercive-field recovery is investigated by illuminating the crystal during the recovery time t_r. Green light from a Nd:YAG laser ($\lambda = 532\,\mathrm{nm}$) and UV light from an Ar-ion laser ($\lambda = 355\,\mathrm{nm}$) is used.

3 Results

When a voltage U is provided by the high-voltage power supply, the voltage applied to the crystal U_K depends on the displacement current i that is limited due to the safety resistor ($50\,\mathrm{M\Omega}$) and Ohm's law ($U_K = U - Ri$). Figure 3 shows a typical displacement current when the crystal is poled with a linear voltage ramp (applied voltage $U \propto t$): U_K and the displacement current i are plotted vs. the time t in which the voltage is ramped. At a certain time, the poling process starts and a displacement current i arises. The spiky behavior of i is striking. The poling process continues for approximately 20 s. The displacement current drops to zero when the whole connected area has been poled. This sudden drop can be used as a precise definition of the end of poling, and the applied voltage U at this time yields the coercive field. All coercive fields that are given in the following are determined according to this procedure. It is evident that due to the safety resistor there might be a systematic overestimation of E_c. However, the interest is focused on the dynamics and on the influence of illumination on the recovery of the coercive field after a poling event. E_c determined by the method described above is very useful for this purpose because of the high reproducibility, which is about 1 per cent.

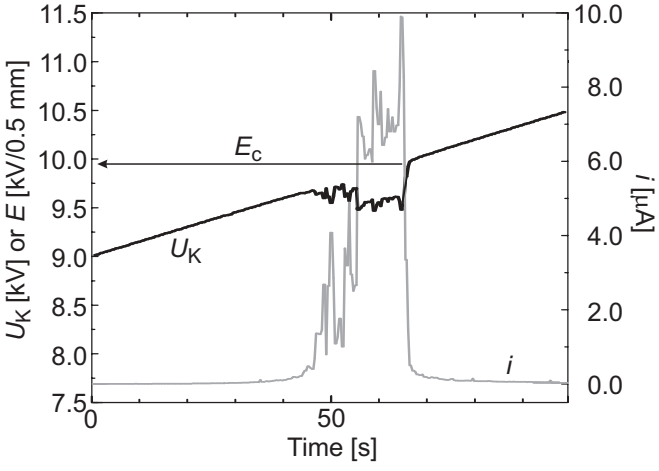

FIGURE 3 Displacement current i and voltage U_K applied to the crystal vs. time t. The voltage U is being ramped linearly with time. When the poling starts ($t \approx 60\,\mathrm{s}$) the displacement current causes a drop of the voltage at the safety resistor $R = 50\,\mathrm{M\Omega}$. Therefore the voltage at the crystal U_K is reduced: $U_K = U - Ri$. The poling starts at a voltage of approximately $U_K = 9.7\,\mathrm{kV}$ and continues for approximately 20 s. When the whole contacted area is poled, the displacement current suddenly drops to zero

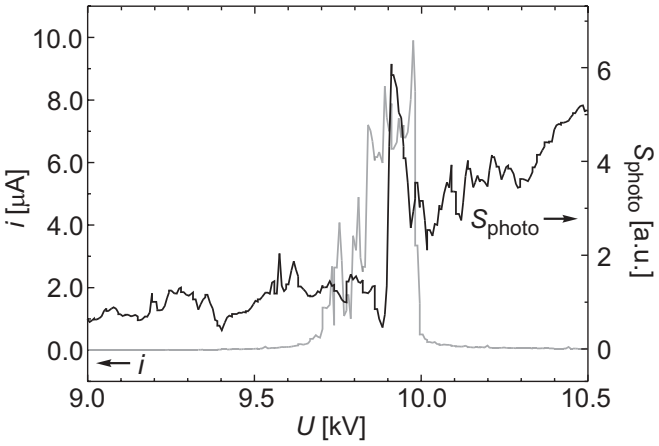

FIGURE 4 Interference effect observed by the photodiode during a poling process. This figure shows the same poling experiment as in Fig. 3, but here the displacement current i and the photodiode signal S_{photo} are plotted vs. the applied voltage U. While the displacement reveals only the integrated behavior of the process, the intensity at a single spatial point of the crystal shows a discontinuity when the domain direction is flipped at this position

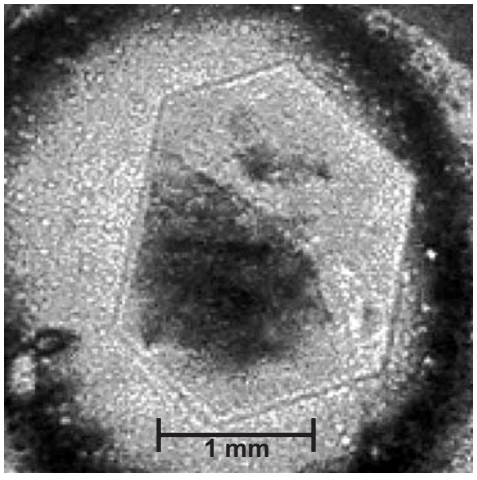

FIGURE 5 Observation of the screen (see Fig. 2) resolves the whole spatial dynamics of a poling process. The picture shows the situation approximately 7.5 s after the beginning of the poling. Besides the interference rings, the picture reveals a hexagonally shaped discontinuity, which represents the domain walls

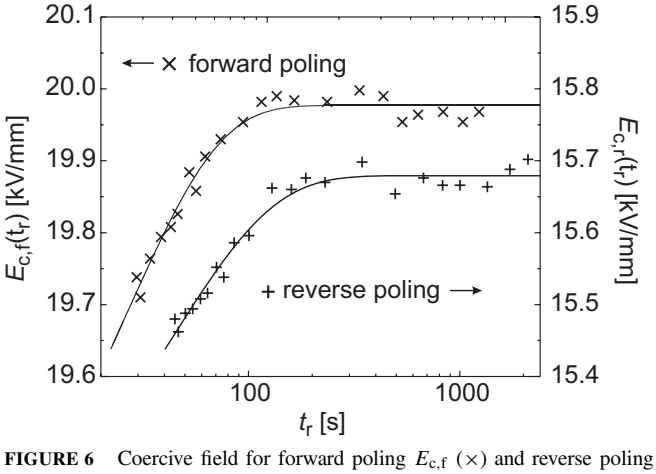

FIGURE 6 Coercive field for forward poling $E_{\text{c,f}}$ ($\times$) and reverse poling $E_{\text{c,r}}$ ($+$) vs. the recovery time t_{r} since the previous poling. The recovery shows an exponential behavior: $E_{\text{c}}(t_{\text{r}}) = E_{\text{c0}} - A\exp(-t_{\text{r}}/\tau)$. The *symbols* show the measured data and the *solid lines* are fits according to this equation

Poling direction	E_{c0} (kV/mm)	A (kV/mm)	τ (s)
Forward	19.978 ± 0.004	0.77 ± 0.09	27 ± 3
Reverse	15.680 ± 0.006	0.62 ± 0.05	39 ± 5

TABLE 1 Obtained fit parameters for the recovery of the coercive field in forward and reverse directions: $E_{\text{c}}(t_{\text{r}}) = E_{\text{c0}} - A\exp(-t_{\text{r}}/\tau)$

In addition, the intensity of the interference pattern at the photodiode position is measured (see Fig. 2). Figure 4 shows the same poling experiment as in Fig. 3, but now the intensity signal S_{photo} of the photodiode and the displacement current i are plotted vs. the applied voltage U. The photodiode monitors the interference-light intensity at a single point of the crystal. The discontinuity in the intensity signal (at $U = 9.9$ kV) corresponds to the poling of the crystal at this position.

Observation of the whole interference pattern on the screen reveals the spatial dynamics of the poling process: at a certain voltage the poling begins at some small starting points, distributed randomly over the crystal. These inversion seeds then grow along certain preference axes with a threefold symmetry. Figure 5 shows one frame of the obtained poling movie. A poled area can be seen clearly as a hexagon-

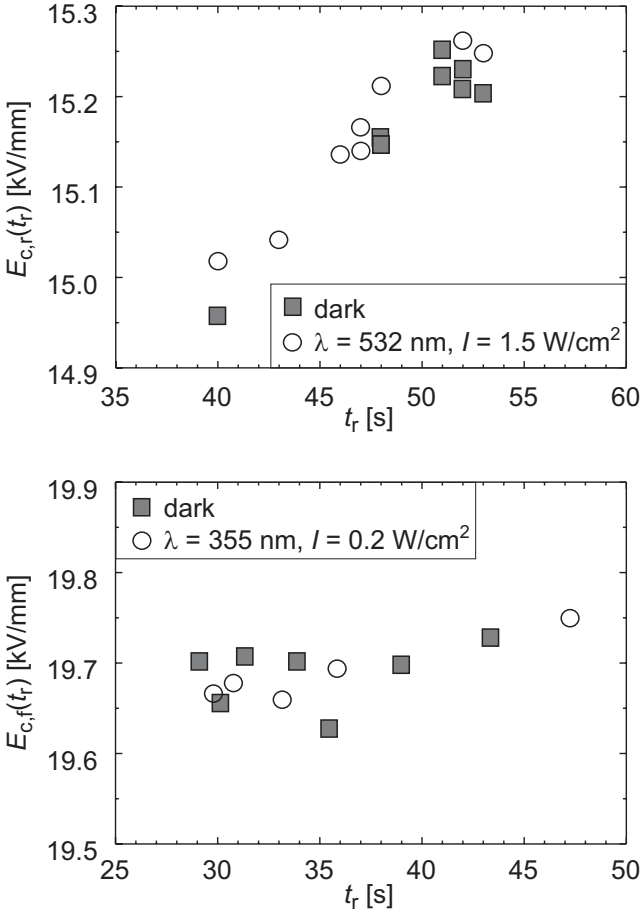

FIGURE 7 Both graphs show the coercive field E_{c} vs. the recovery time t_{r} since the last poling. The possible influence of green ($\lambda = 532$ nm, *upper graph*) and ultraviolet light ($\lambda = 355$ nm, *lower graph*) on the recovery of the coercive field is investigated ($E_{\text{c,r}}$ and $E_{\text{c,f}}$ are coercive fields for reverse and forward poling, respectively)

shaped discontinuity within the interference rings. Growth of the poled areas happens step-wise during the 20-s poling period.

Figure 6 shows the coercive fields in forward and reverse directions, $E_{c,f}$ and $E_{c,r}$, vs. the recovery time t_r between two successive domain inversions. The recovery of E_c shows an exponential behavior of the form $E_c(t_r) = E_{c0} - A\exp(-t_r/\tau)$, as suggested in related works for $LiNbO_3$ [12] and $LiTaO_3$ [9, 10]. The obtained fit parameters are given in Table 1.

In further experiments the influence of green ($\lambda = 532$ nm, $I = 1.5\,W/cm^2$) and ultraviolet light ($\lambda = 355$ nm, $I = 0.2\,W/cm^2$) on the coercive-field recovery is investigated. The crystal is illuminated for the whole recovery time t_r. Figure 7 shows the results for small t_r, when the effect of light is expected to be maximal. As an example the influence of ultraviolet light on the forward-poling recovery (upper graph) and of green light on the reverse-poling recovery (lower graph) is shown. There is obviously no significant influence of the illumination on the coercive-field recovery.

4 Discussion

The homogeneous electrical contact with water as a liquid electrode is convenient for reproducible poling experiments, and the transparency of the electrodes enables us to investigate light-induced effects.

Observation of the displacement current gives first information about the dynamics of the poling process and it allows a precise definition of the end of poling. However, this method shows a major disadvantage: it only reveals the integrated behavior of the poling process over the whole electrode area.

The electro-optic interferometric observation method gives information about the spatial dynamics of the poling. The intensity signal in Fig. 4 shows a discontinuity, which corresponds to domain inversion at the observed point. This discontinuity is easily explained: the domain inversion causes a change of sign of the tensor element r_{13} and therefore the electro-optically induced refractive-index change switches sign. Observation of the interference pattern reveals a domain growth corresponding to the three-fold rotation symmetry of the crystal. The domain walls are preferably oriented along the crystal axes. This effect must be considered for domain patterning. The temporal dynamics of the poling process is mainly explained by the high safety resistance: because of the high displacement current the voltage applied to the crystal U_K drops according to Ohm's law. When the electric field falls below the coercive field, the poling itself stops, the displacement current vanishes and the electric field can be built up again. This repetitive process explains the spiky displacement current in Fig. 3 as well as the relatively long duration of the whole poling. Together with the preferred domain-wall orientation, the step-wise growth of the domains is also explained by the repetitive reduction and increase of the electric field. This interferometric method can be utilized for in situ observation of poling experiments. Using an appropriate magnification, it is feasible to use it for online control of domain patterning.

After a domain inversion the coercive field E_c shows a transient reduction. It can be approximated by $E_c(t_r) = E_{c0} - A\exp(-t_r/\tau)$ as suggested in related literature [9, 10, 12]. This effect is differently pronounced for forward and reverse directions. The time constants are determined to be $\tau = (27 \pm 3)$ s for $E_{c,f}$ and $\tau = (39 \pm 5)$ s for $E_{c,r}$. Our results show a substantially faster coercive-field recovery than has been reported in other articles: Wang et al. measure time constants twice as long, using high-voltage pulses for poling [12]. However, their method does not allow direct observation of the poling process. Yet another behavior of the coercive-field recovery is found in an associated work, investigating very short recovery times: Ro and Cha describe a stretched exponential recovery, also using an indirect observation method [13]. In any case the coercive-field recovery in $LiNbO_3$ is much faster than in $LiTaO_3$, which shows a recovery time constant of $\tau \approx 140$ s [11]. This fast recovery makes investigations of the influence of light on E_c more difficult than in $LiTaO_3$.

The influence of both green ($\lambda = 532$ nm) and UV light ($\lambda = 355$ nm) has been investigated (Fig. 7). Only for short recovery times are the processes investigated, since the effect of light is supposed to be maximal for this period. However, no influence of light on the coercive-field recovery was observed.

5 Conclusions

We demonstrated an electro-optic interferometric in situ observation method for poling experiments with lithium niobate, which is suitable for online control of domain patterning. The observed dynamics of domain inversion shows that the domain walls are preferentially aligned along the crystal axes. We measured a transient reduction of the coercive field with an exponential recovery, which is the major requirement for future light-induced domain patterning. However, so far no influence of illumination on the recovery of the coercive field was observed. Further experiments, especially with shorter recovery times and higher light intensities, have to be performed to clarify whether light-frustrated poling in lithium niobate is possible.

ACKNOWLEDGEMENTS Financial support by the DFG and the Deutsche Telekom AG is gratefully acknowledged.

REFERENCES

1 E.J. Lim, M.M. Fejer, R.L. Byer, W.J. Kozlovsky: Electron. Lett. **25**, 731 (1989)
2 M.M. Fejer, G.A. Magel, D.H. Jundt, R.L. Byer: IEEE J. Quantum Electron. **QE-28**, 2631 (1992)
3 G.A. Magel, M.M. Fejer, R.L. Byer: Appl. Phys. Lett. **56**, 108 (1990)
4 L.E. Myers, R.C. Eckardt, M.M. Fejer, R.L. Byer, W.R. Bosenber, J.W. Pierce: J. Opt. Soc. Am. B **12**, 2102 (1995)
5 M. Houé, P.D. Townsend: J. Phys. D: Appl. Phys. **28**, 1747 (1995)
6 M. Yamada: Rev. Sci. Instrum. **71**, 4010 (2000)
7 R.G. Batchko, V.Y. Shur, M.M. Fejer, R.L. Byer: Appl. Phys. Lett. **75**, 1673 (1999)
8 J.P. Meyn, M.M. Fejer: Opt. Lett. **22**, 1214 (1995)
9 S. Chao, W. Davis, D.D. Tuschel, R. Nichols, M. Gupta, H.C. Cheng: Appl. Phys. Lett. **67**, 1066 (1995)
10 S. Chao, C. Hung: Appl. Phys. Lett. **69**, 3803 (1996)
11 P.T. Brown, G.W. Ross, R.W. Eason, A.R. Pogosyan: Opt. Commun. **163**, 310 (1999)
12 H.F. Wang, Y.Y. Zhu, S.N. Zhu, N.B. Ming: Appl. Phys. A **65**, 437 (1997)
13 J.H. Ro, M. Cha: Appl. Phys. Lett. **77**, 2391 (2000)